Geophysical Research Letters

RESEARCH LETTER
10.1029/2018GL079894

Contrasting Mechanisms of Summer Blocking Over Western Eurasia

Marie Drouard[1] **and Tim Woollings**[1]

[1] Atmospheric, Oceanic and Planetary Physics, University of Oxford, Oxford, UK

Key Points:
- Contrasting roles of high- and low-frequency processes over southern central Europe and western Russia
- Jet exit location contribution to blocking formation in southern central Europe by forcing descent in the block area
- Risk of extreme seasons cannot be estimated easily based on statistics of past events alone

Supporting Information:
- Supporting Information S1

Correspondence to:
M. Drouard,
marie.drouard@physics.ox.ac.uk

Citation:
Drouard, M., & Woollings, T. (2018). Contrasting mechanisms of summer blocking over western Eurasia. *Geophysical Research Letters*, *45*, 12,040–12,048. https://doi.org/10.1029/2018GL079894

Received 3 AUG 2018
Accepted 25 OCT 2018
Accepted article online 31 OCT 2018
Published online 9 NOV 2018

Abstract The formation of summer blocking events appears to have been mostly studied for a few individual events often associated with heat waves. Here we investigate summer blocking event dynamics in three areas over western Eurasia in order to draw some more general conclusions, mostly in terms of high- and low-frequency processes. A 2-D blocking event detection algorithm is applied to the 500-hPa-geopotential field from the ERA-40 and ERA-Interim reanalyses over the 1958–2017 period. It is shown that both high- and low-frequency processes are important to initiate blocking events over southern central Europe. Blocking events over western Russia are preceded by a significant low-frequency large-scale wave train, and their formation and maintenance are dominated by low-frequency processes only. Finally, it is shown that the risk of extreme seasons such as summer 2010 cannot be accurately estimated from the Poisson statistics of past events.

Plain Language Summary Atmospheric blocking events correspond to a large-scale reversal of the meridional pressure gradients that blocks the eastward propagating jet stream. In an atmospheric pressure chart, they are characterized by a large-scale high-pressure system. Blocking events strongly impact the weather mainly because of their persistence (up to 4–5 weeks), which allows anomalies in temperature to amplify. Because of their long persistence, they can be associated in summer with heat waves, which have major societal impacts (as in June 1976 in the UK, August 2003 in France, or July–August 2010 over eastern Europe and Russia). Blocking events dynamics has been less studied in summer than in winter, partly because of the smaller occurrence of blocking events in summer. Here we address the dynamical processes involved in summer blocking events over the European-western Russia region (where the 1976, 2003, and 2010 blocking events occurred) to better understand what the key ingredients for their formation and dynamics are. To do that, we looked at blocking events in observations in summer over three key areas in the European-western Russia area. We show that western Russia is particularly prone to very long, high-impact blocks due to the nature of the atmospheric fluid dynamics that influences that region.

1. Introduction

Atmospheric blocking is a phenomenon of major importance as it strongly impacts the daily weather due to its long persistence (up to 4–5 weeks). It corresponds to a localized large-scale reversal of the atmospheric circulation that blocks the zonal flow (Rex, 1950).

Several mechanisms have been proposed to contribute to block formation, for instance, large-scale Rossby wave dynamics (e.g., Austin, 1980; Charney & Devore, 1979; Egger, 1978; Legras & Ghil, 1985), rapid cyclogenesis (Colucci, 1985; Nakamura & Huang, 2018; Rivière & Orlanski, 2007; Sanders & Gyakum, 1980), forcing by anomalies in the tropics (Cassou et al., 2005; Hoskins & Sardeshmukh, 1987), or more recently the contribution of latent heat release (Pfahl et al., 2015). There is no consensus on a unique mechanism of blocking formation (Woollings et al., 2018), with evidence that a different balance of mechanisms can occur in different cases. For example, Nakamura et al. (1997) showed for winter circulation that the contribution of high- and low-frequency forcings varies regionally.

Summer blocking events are increasingly studied as long persistent events can be associated with very high temperatures and heat waves (Della-Marta et al., 2007; Green, 1977; Schaller et al., 2018; Sousa et al., 2018). This was the case during the 2010 summer over Russia. That summer was marked by an exceptional succession of blocking events that affected the region for the major part of the summer (Matsueda, 2011; Schneidereit et al., 2012). This led to an unprecedented strong heat wave over the area (Barriopedro et al., 2011;

Galarneau et al., 2012; Miralles et al., 2014). Schneidereit et al. (2012) showed that the transition toward a La Niña phase in the eastern tropical Pacific influenced the formation and maintenance of the blocks by the propagation of a low-frequency large-scale Rossby wave train. On the other hand, Green (1977) showed that stationary large-scale Rossby waves alone could not explain the structure and maintenance of the west European block of July 1976 and instead highlighted the necessity of transient eddies contribution.

The literature described above suggests that different mechanisms might dominate in western Europe and western Russia, so our focus is on comparing these regions to determine whether these differences in mechanisms hold for blocking in general. The data and blocking detection algorithm are introduced in section 2. Results are presented in section 3 and discussed in section 4.

2. Data and Method

Our analysis is based on the four times daily reanalysis data combining ERA-40 (Uppala et al., 2005) and ERA-Interim (Dee et al., 2011) from the European Centre for Medium-Range Weather Forecasts on a 0.75° × 0.75° grid. We only consider summer months from June to August for the period 1958–1978 from ERA-40 and 1979–2017 from ERA-Interim. Several fields were used, in particular geopotential at 500 hPa (Z500), zonal and meridional winds at 300 hPa (U300 and V300, respectively), and potential vorticity (PV) at 330 K (only for the ERA-Interim period as it is not available for ERA-40). Daily averages were computed for all the data. Anomalies were computed by subtracting the monthly climatologies from the total field. To finish, some fields were decomposed into high- and low-frequency parts, using a Lanczos filter with a cutoff period of 7 days, to separate the synoptic-scale signal from that of the low-frequency part (Duchon, 1979).

2.1. Detection of Atmospheric Blocking Events

Blocking events in the atmosphere are identified using the 2-D method developed by Masato et al. (2013), which searches for persistent and large-scale reversals of the meridional gradient of Z500 lasting at least 5 days. The details of the blocking event computation are given in the supporting information (Text S1).

The climatology of the repartition of blocking days (Figure S1 in the supporting information) is very similar to that obtained by Masato et al. (2013) for ERA-40. Over Europe, it shows a clear maximum in blocking days at around 30°E. Here we focus on the events located on the western and eastern edges of this maximum where the 2003 and 2010 heat waves occurred respectively and compare them to those located over the center.

2.2. Blocking Event Area Indices

We constructed three indices that are equal to one when a blocking center on onset day is located in a given area. They are delimited as follows:

- Western area: 0–20°E, 40–50°N for southern central Europe (dots in Figure 1d);
- Central area: 20–40°E, 50–60°N where there is a climatological maximum of blocked days (dots in Figure 1e);
- Eastern area: 35–55°E, 45–55°N for western Russia (dots in Figure 1f).

Composites of the Z500, zonal and meridional winds at 300hPa, etc., were then computed for each of these indices. Lag 0 in the composites represents the onset day of the blocking events whose blocking centers are located in one of the three areas. In total, 15, 57, and 21 blocking events occur in the western, central, and eastern areas, respectively. Despite these varied and small number of events, the composites show a clear and significant blocking signal and clear differences between the three areas. In the eastern area, the algorithm detects three blocking events during the summer 2010, which are associated with the 2010 heat wave in western Russia.

2.3. Q Vectors

Q vectors are computed at 700 hPa to show the location of upward and downward motions related to the jet and future block during the formation stage of the block. These are computed as follows (Hoskins et al., 1987):

$$\mathbf{Q} = (Q_1, Q_2) = \left(-\frac{g}{\theta_0}\frac{\partial \mathbf{V}_g}{\partial x}.\nabla\theta, -\frac{g}{\theta_0}\frac{\partial \mathbf{V}_g}{\partial y}.\nabla\theta\right) \quad (1)$$

where g is the standard gravity, θ the potential temperature, θ_0 the reference value of potential temperature, and $\mathbf{V_g}$ the geostrophic wind vector. The convergence (divergence) of **Q** vectors shows areas of upward (downward) motion. We plot **Q** vectors and not the vertical velocity because it directly informs us where the jet and the potential temperature gradients force vertical motion.

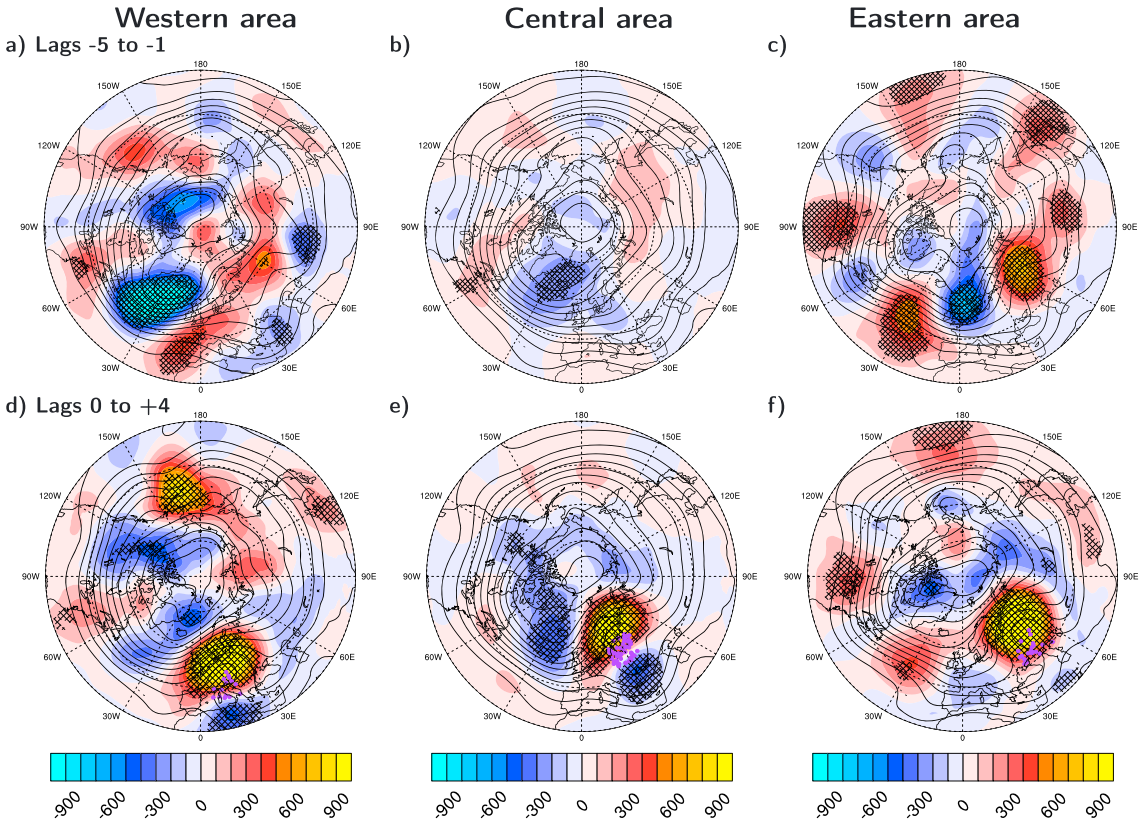

Figure 1. Five-day composites of the Z500 (black contours starting at 52,800 m^2/s^2 with an interval equal to 500 m^2/s^2) and Z500 anomaly (shading in m^2/s^2) for the three areas averaged over the 5 days preceding the onset (a–c) and over the five following days (onset day included; d–f) in June–August 1958–2017 in ERA-40/ERA-Interim. Black stippling represents the 99% confidence level in absolute value calculated with a bootstrapping method. Purple dots (bottom row) show the blocking event locations on the onset day.

3. Results

3.1. Summer Blocking Events Between 1958 and 2017

Five-day composites of the Z500 and Z500 anomaly fields starting on the onset day (Figures 1d–1f) show that the western and central area blocks are dominated by *anticylonic-reversal* situations (see Z500 contours) with a strong high to the north of a weaker low, whereas in the eastern area an Ω-*shaped* structure stands out in the composite indicating the more frequent occurrence of Ω-shaped blocks.

During blocking events there is a negative anomaly in high-frequency kinetic energy over the block area and a northward shift of the storm track (positive anomalies to the north of the block on Figures 2d–2f). The zonal wind appears split: in the central and eastern cases, the Atlantic jet merges with the subtropical jet and another area of strong westerly wind forms on the northern flank of the block; in the western case, the Atlantic jet is largely shifted to the north of the block and a split jet structure appears with the Atlantic jet to the north and the subtropical jet to the south of the block.

3.2. Formation of the Blocking Events

In the western area, blocking events are preceded by a significant large-scale trough anomaly over the North Atlantic (Figure 1a) and the Atlantic jet and storm track are both shifted to the north on the eastern part of the Atlantic basin (Figure 2a). These events seem to develop in the presence of a strong North Atlantic storm track (see positive anomalies over the North Atlantic and in the block area). A further mechanism may contribute to the formation of the block: the jet exit region is located just to the north of the future block, which forces downward (upward) motion on the southern (northern) flank of the jet in the western area as shown by the **Q** vectors (vectors on Figure 2a). This descending air in the area where the block later develops could reinforce the positive Z500 anomaly that develops there. Thus, the northward shifted jet could participate in the forcing of the block in that area.

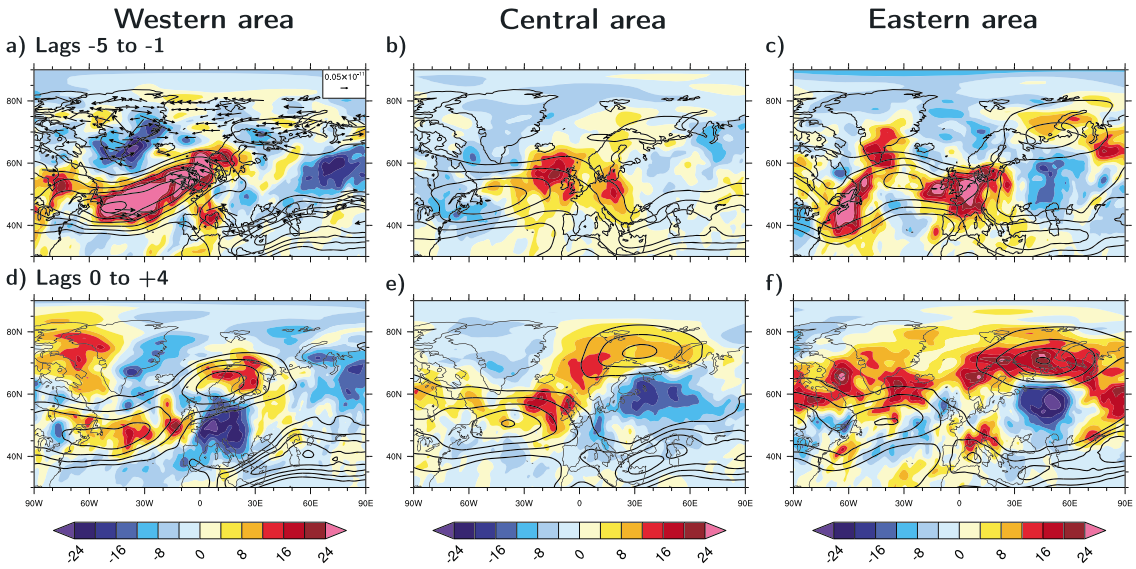

Figure 2. As in Figure 1 but for the high-frequency kinetic energy anomaly (shadings in m^2/s^2) and the zonal wind (black contours starting at 10 m/s with an interval of 4 m/s). Vectors on panel (a) represent the **Q** vectors. **Q** vectors greater than 0.15e−11 are not shown.

In the eastern area, blocking events are preceded by a statistically significant low-frequency wave train (Figure 1c). This is in good agreement with Schneidereit et al. (2012), who showed that the 2010 blocking highs over Russia were associated with a low-frequency wave train likely forced by a La Niña event in the tropical Pacific (see also O'Reilly et al., 2018). We go further by showing that this low-frequency Rossby wave train was not only present during the 2010 events, as we obtain the same results when the blocking events of summer 2010 are removed (Figure S2 in the supporting information; the same holds for 2003 in the western area). This implies that this low-frequency wave train is a strong driver of blocking events in the eastern area. It is associated with a positive Z500 anomaly in the location of the block indicating that the area is already dominated by anticyclonic flow before the onset. This is in good agreement with the negative high-frequency kinetic energy anomaly observed in the days before the onset in the eastern area (Figure 2c).

Five-day composites prior to blocking events in the central area do not show any significant signal (Figure 1b). Indeed, some events are preceded by a negative geopotential anomaly as for the western case, some by a low-frequency wave train as in the eastern case, and other events by neither of these two patterns (not shown). We nevertheless find it valuable to study blocks in that area, as they allow us to draw better statistics and form a useful comparison to the western and eastern cases.

To conclude, the dynamics associated with the western and eastern events appears to be very different and the high-frequency transients may play a less dominant role in the eastern events compared to western events. This is the hypothesis that we investigate in the following analysis.

3.3. Role of the High- and Low-Frequency Transients

In the following, we used the PV at 330 K to investigate the role of high- and low-frequency transient flows during block formation (as in Illari, 1987). Figures 3a–3c show the evolution of the PV anomaly zonally averaged within the three areas. In the western and central areas, it becomes strongly negative only 1 day before the onset (Figures 3a and 3b) showing that the block formation was very rapid. In the eastern area, there is already a negative PV anomaly 8 days before the onset (Figure 3c).

Mullen (1987) showed that the transient eddy vorticity flux forcing was located one quarter of wavelength upstream of the block. Therefore, we investigated the contribution of the high- and low-frequency transients upstream of the block. To do that, we looked at the transient part of the time-averaged PV equation (Illari, 1987):

$$\overline{\mathbf{v}}.\nabla\overline{q} + \nabla.\overline{(\mathbf{v}'q')} = 0. \tag{2}$$

where q represents the PV field, overbar denotes the time-averaged quantity, and primes the deviation from this time average. The transient part corresponds to the divergence of the anomalous PV fluxes. Here we

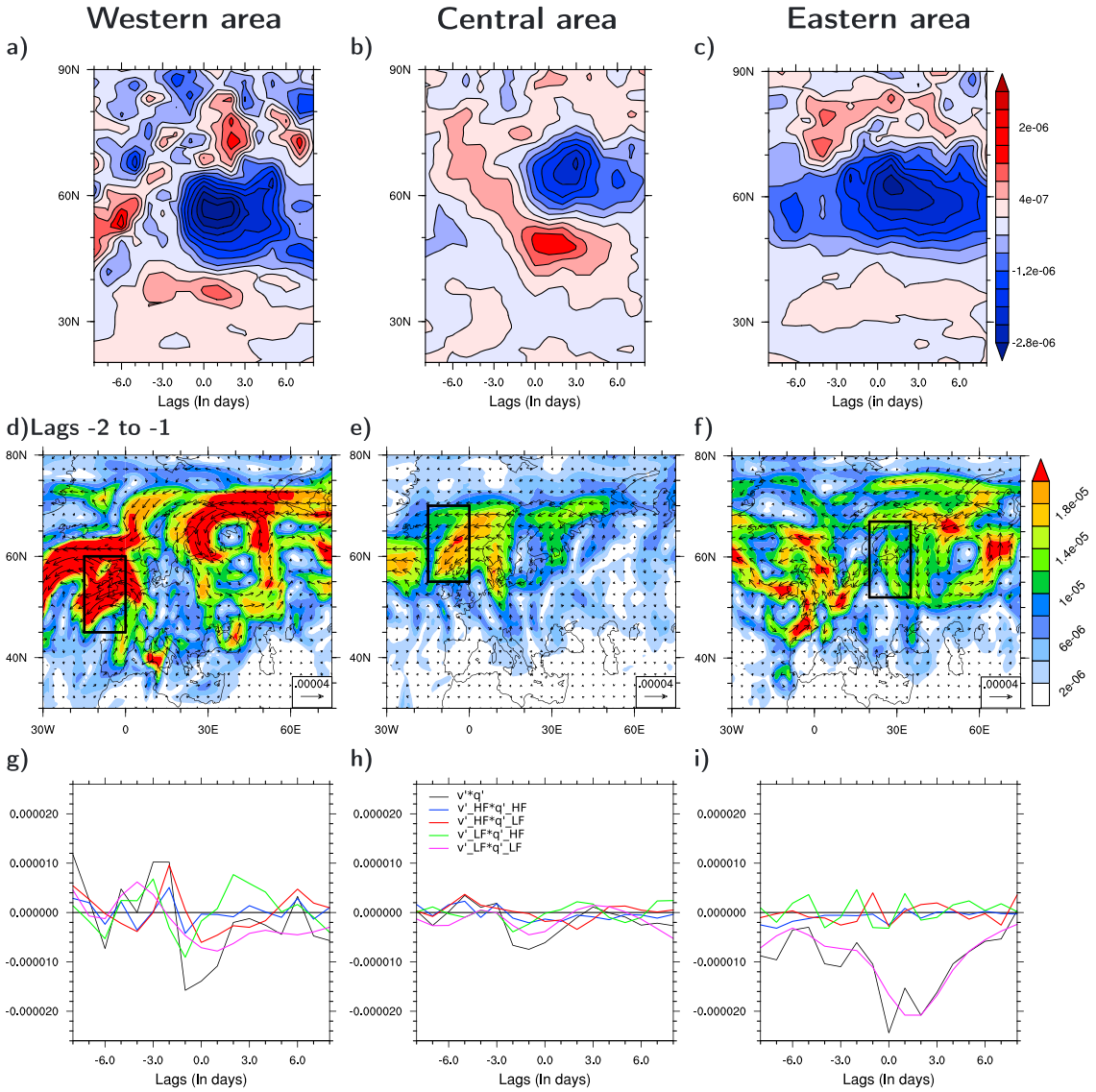

Figure 3. (a–c) Time evolution of the zonally averaged 330-K-potential vorticity (PV) anomaly in the three areas (in $m^2 \cdot s^{-1} \cdot K \cdot kg^{-1}$). (d–f) Time average of the 2 days preceding the onset of the composites of the anomalous PV fluxes ($\mathbf{u}'PV'$; arrows; see scale at bottom in $m^3 \cdot s^{-2} \cdot K \cdot kg^{-1}$) and intensity of the anomalous PV fluxes (color shadings in $m^3 \cdot s^{-2} \cdot K \cdot kg^{-1}$) at 330 K. (g–i) Time evolution of the composite of the anomalous meridional PV fluxes at 330 K averaged in the black boxes shown in Figures 3d–3f ($v'PV'$ in $m^3 \cdot s^{-2} \cdot K \cdot kg^{-1}$). *HF* and *LF* in Figure 3h stand for high and low frequency, respectively. These computations are made over the ERA-Interim period only (1979–2017). Over that period, there are 6, 32, and 15 blocking events in the western, central, and eastern areas, respectively.

present the PV fluxes rather than their divergence as the field is smoother. Anomalous PV fluxes are perfectly suitable to study the relative contribution of the high- and low-frequency transients.

Upstream of the three areas, anomalous PV fluxes are negative over the 2 days preceding the block formation (black boxes on Figures 3d–3f). In the eastern area, anomalous PV fluxes on the upstream side are meridional as there is already an anticyclone in the blocking area before the onset (Figure 3f). For the two other cases, anomalous PV fluxes appear mostly NE-SW oriented (see black boxes in Figures 3d and 3e), consistent with low PV air moving northeastward from the subtropics (see Figure S3 in the supporting information).

We decomposed the anomalous PV fluxes into high- and low-frequency contributions (Text S2 in the supporting information). We averaged these in an area located upstream of the block (black boxes in Figures 3d–3f) and look at their time evolution in Figures 3g–3i. Here we only show the composites of the meridional anomalous fluxes as the zonal anomalous fluxes from 8 days before the onset to 4 days after the onset are always negative (not shown). Meridional anomalous fluxes show stronger variations and their sign and intensity are

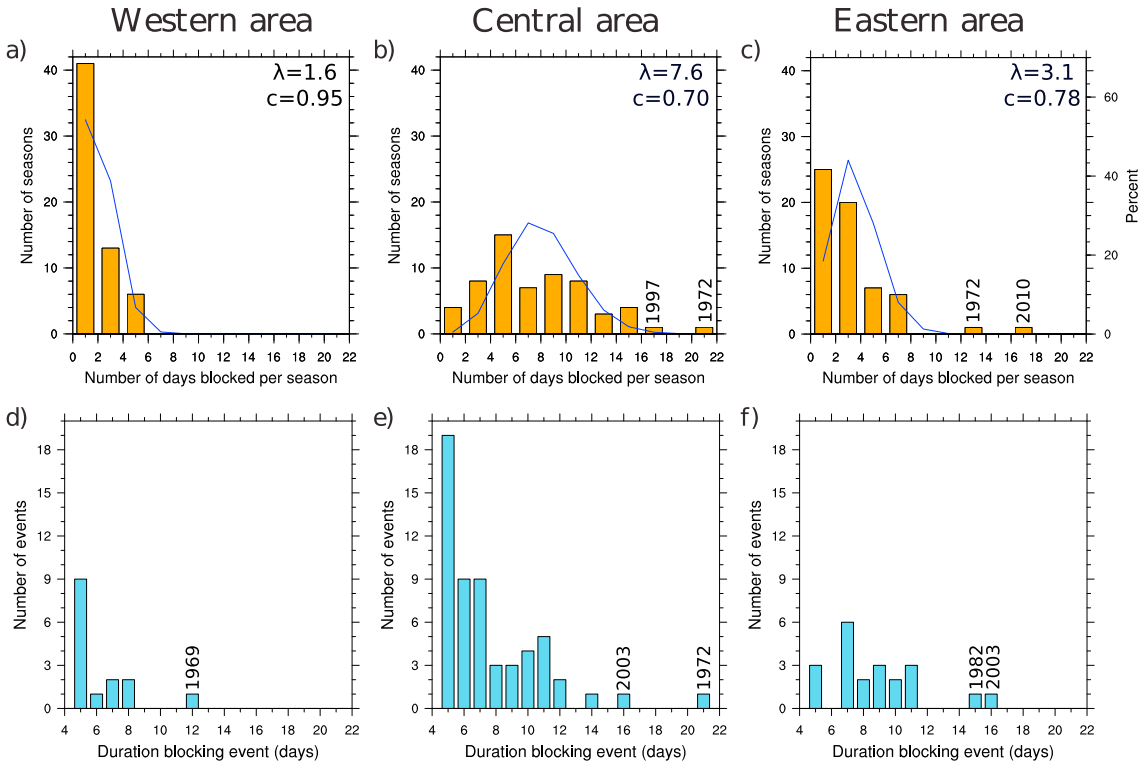

Figure 4. (a–c) Number of summers as a function of their number of blocked days averaged over each area (yellow bars). Each bar represent the number of summers with an average number of blocked days greater than or equal to 0 (2, 4, …) and less than 2 (4, 6, …) days. The blue curves show the Poisson distribution applied to describe how the area is impacted by blocks for a given number of days (0, 1, 2, 3, …) per summer. The λ value (time-averaged number of blocked days per summer per area) is shown on each panel. c is the correlation between the area-weighted average number of blocked days per season and the Poisson distribution. (d–f) Number of events as a function of their duration. Numbers on top of a column indicate the year of the blocking event (d–f) or of the summer (a–c).

good proxies for the formation and amplification of the anticyclone. Note that this diagnostic is strongly affected by noise and the significance of any individual point is low (the spread between events is of the order of 1.5 $\times 10^{-5}$ $m^3 \cdot s^{-2} \cdot K \cdot kg^{-1}$). Despite this, clear qualitative differences in the evolution are apparent between the regions. In the eastern area, total meridional anomalous PV fluxes are clearly dominated by the transport of low-frequency PV air by the low-frequency meridional wind (compare magenta and black curves in Figure 3i). Moreover, as expected, the meridional anomalous PV fluxes are already negative 8 days before the onset day. The marked drop observed 1 day before the onset is then a marker of the strong amplification of the ridge and the circulation associated with it.

In the western area, we also observe a drop in the values of the total meridional anomalous PV fluxes, which become suddenly negative one day before the onset (black curve on Figure 3f). Before that, we see strong variations in the PV fluxes in that area that testify to the propagation of synoptic system over the area (see variations in the black curve). This sudden and strong change seems to be due to the transport of high-frequency PV air by the low-frequency meridional wind (green curve) in large part. The transport of high-frequency PV air by the high-frequency meridional wind (blue curve) and transport of low-frequency PV air by the low-frequency meridional wind (magenta curve) also make a lesser contribution. This implies that block formation is due to the combination of a synoptic system and low-frequency ridge.

Then, once the block is formed, the low-frequency PV terms become stronger and participate in the maintenance of the block over the following 5 days (red and magenta curves, respectively). The transport of high-frequency PV air by the high-frequency meridional wind (blue curve) becomes very small after onset, which can be explained by the fact that the storm track is shifted northward. Thus, the high- and low-frequency transients seem to both play an important role in the western area at different periods of the block life cycle. A similar succession also happens in the central area but with a weaker signal. To conclude,

the low-frequency transients dominates the formation of the blocks in the eastern case, whereas both high- and low-frequency transients contribute to it in the western case.

3.4. Duration

Here we look for differences in the duration of blocking events, which may relate to differences in mechanisms identified. In the western area, there are mainly short blocking events and only one long event (Figure 4d). On the contrary, in the eastern area, there are both long-lasting and short-lasting events with a few very long-lasting events making blocking events in average longer in that area than in the western area (Figure 4f). Comparison of Figures 4e and 4f highlights the unusually high occurrence of long events in the eastern area given the number of short events.

Figures 4a–4c show the distribution of the number of days blocked per summer averaged over each area (yellow bars; see Text S1 in the supporting information for details on the computation) and a Poisson distribution applied to describe the chance for the area to be impacted by blocking for a certain number of days per summer. Individual event duration is not sufficient to infer how an area is impacted by blocking events during a summer; hence, we computed the area-weighted average number of blocked days per summer, which is easily related to seasonal drought and heat wave. We also compute the Poisson distribution to attempt to model the distribution of blocked days per summer in each area. In the eastern area, most of the blocking events are long but sporadic as the area-weighted average number of blocked days is less than 4 days per summer. The 2010 blocking events do not stand out individually in terms of duration (one event of 7 days and two of 10 days; see Figure 4f), but the succession of these three events caused the area to be blocked for an exceptionally long time. In the central area, the multiple 5-day blocks seem to have a greater impact (than the few long events of the eastern area) as the maximum number of summers is around four to height days blocked per summer. The western area shows a distribution of days blocked more similar to that of the duration of the blocking events. Indeed, there are only 15 events and most of them are short, so there is only a small number of days blocked per summer.

It is interesting to see that Poisson distribution appears to be relevant to describe the number of times that the areas are impacted by blocking for a given number of days per summer (see correlations on Figure 4). The Poisson distribution clearly shows that the distribution of blocked days is expected to be wider in the central area than in the western and eastern areas. However, the Poisson distribution predicts a very low probability that they are more than 11 blocked days per summer in average in the eastern area. This emphasizes that the 2010 succession of blocking events was exceptional. This also explains the lower value of the correlation between the data and the Poisson distribution (see Figure 4). On the contrary, summers with an average of up to 17 blocked days are to be expected in the central area. This shows that some summers with high blocking occurrence are to be expected in the central region where the climatological occurrence is the highest. To finish, the exceptionally long period of blocked days in 1972 is related to one exceptionally long blocking event (21 days) that induced the 1972 heat wave over Finland (Russo et al., 2015) and was apparently responsible for some of the blocked days over the eastern area (Figure 4c).

To conclude, the average number of days blocked in the area is not always enough to quantify the risk of experiencing a summer of high blocking occurrence. Applying the Poisson distribution shows that in the eastern and to a lesser extent the central regions, summers with extremely frequent blocking have occurred and these were not to be expected based on the climatological frequency there.

4. Summary and Discussion

Here we studied the formation and characteristics of blocking events in three areas over western Eurasia. In the western area, PV transport by high- and low-frequency winds is responsible for the initial formation of the block and the transport of low-frequency PV acts then to reinforce and maintain the block once it is formed. High-frequency flow may also contribute to the maintenance of the flow by reinforcing the Atlantic jet northward of the block as in Berckmans et al. (2013). We additionally suggest that dynamically forced descent associated with the jet exit over Europe may contribute to the development of blocks here.

On the contrary, blocking events in the eastern area appear to be triggered and maintained by the low-frequency flow. These events are statistically significantly preceded by a large-scale low-frequency Rossby wave train possibly originating in the North Pacific, which is in very good agreement with the study of Schneidereit et al. (2012) for the 2010 summer. Our results show that the individual blocking events in 2010

were not exceptional in terms of dynamics compared to the other events occurring in that area but that the succession of the three events makes the summer exceptional in terms of blocked days. Indeed, the extreme summers in this area stand out as being inconsistent with a simple Poisson model, suggesting distinct seasonal dynamics or a distinct driver such as El Niño–Southern Oscillation or the combination of two drivers (as shown by Schneidereit et al., 2012) compared to the other seasons.

Blocking events in the central area are located at the end of the storm track. Therefore, different processes act on the western and eastern flanks of that area as shown before and blocking events in the central area appear to be the results of a mix of these.

Problems representing the large-scale low-frequency wave train forcing in general circulation models (e.g., O'Reilly et al., 2018) could lead to an underestimation of blocking events in the eastern area. This could explain the negative bias observed in twentieth century coupled runs from general circulation models from CMIP5 (see Figure 5 from Masato et al., 2013) at 30–50°E, 60°N. Our results also suggest that the behavior of western events in a future climate is more dependent on the storm track changes, while eastern events will depend more on the stationary and low-frequency wave changes.

To conclude, the region on the eastern flank of the Eurasian summer blocking maximum is distinct in being strongly influenced by low-frequency dynamics and less by the storm track. Contrary to what would be expected, this does not suggest a higher level of predictability during a block summer as shown by Matsueda (2011) for the 2010 summer. Moreover, it also seems that the risk of extreme seasons such as this cannot be estimated well based on statistics of past events alone.

Acknowledgments
The authors would like to thank two anonymous reviewers for their constructive comments and suggestions. This work was funded by the NERC project "Robust Spatial Projections of Real-World Climate Change" (NE/N01815X/1). All the data used in this paper were downloaded on the website of the ECMWF: https://www.ecmwf.int/en/forecasts/datasets/archive-datasets/browse-reanalysis-datasets.

References

Austin, J. F. (1980). The blocking of middle latitude westerly winds by planetary waves. *Quarterly Journal of the Royal Meteorological Society*, *106*, 327–350.

Barriopedro, D., Fischer, E., Luterbacher, J., Trigo, R. M., & García-Herrera, R. (2011). The hot summer of 2010: Redrawing the temperature record map of Europe. *Science*, *332*, 220–224.

Berckmans, J., Woollings, T., Demory, M.-E., Vidale, P.-L., & Roberts, M. (2013). Atmospheric blocking in a high resolution climate model: Influences of mean state, orography and eddy forcing. *Atmospheric Science Letters*, *14*, 34–40.

Cassou, C., Terray, L., & Phillips, A. S. (2005). Tropical Atlantic influence on European heat waves. *Journal of Climate*, *18*, 2805–2811.

Charney, J. G., & Devore, J. G. (1979). Multiple flow equilibria in the atmosphere and blocking. *Journal of the Atmospheric Sciences*, *36*, 1205–1216.

Colucci, S. J. (1985). Explosive cyclogenesis and large-scale circulation changes: Implications for atmospheric blocking. *Journal of the Atmospheric Sciences*, *42*, 2701–2717.

Dee, D. P., Uppala, S. M., Simmons, A. J., Berrisford, P., Poli, P., Kobayashi, S., et al. (2011). The ERA-Interim reanalysis: Configuration and performance of the data assimilation system. *Quarterly Journal of the Royal Meteorological Society*, *137*, 553–597.

Della-Marta, P., Luterbacher, J., von Weissenfluh, H., Xoplaki, E., Brunet, M., & Wanner, H. (2007). Summer heat waves over western Europe 1880–2003, their relationship to large-scale forcings and predictability. *Climate Dynamics*, *29*, 251–275.

Duchon, C. E. (1979). Lanczos filtering in one and two dimensions. *Journal of Applied Meteorology*, *18*, 1016–1022.

Egger, J. (1978). Dynamics of blocking highs. *Journal of the Atmospheric Sciences*, *35*, 1788–1801.

Galarneau, T. J. Jr., Hamill, T., Dole, R., & Perlwitz, J. (2012). A multiscale analysis of the extreme weather events over western Russia and northern Pakistan during July 2010. *Monthly Weather Review*, *5*, 1639–1664.

Green, J. S. A. (1977). The weather during July 1976: Some dynamical considerations of the drought. *Weather*, *32*, 120–126.

Hoskins, B. J., Draghici, I., & Davies, H. C. (1987). A new look at the ω-equation. *Quarterly Journal of the Royal Meteorological Society*, *104*, 31–38.

Hoskins, B. J., & Sardeshmukh, P. J. (1987). A diagnostic study of the dynamics of the Northern Hemisphere winter of 1985–86. *Quarterly Journal of the Royal Meteorological Society*, *113*, 759–778.

Illari, L. (1987). A diagnostic study of the potential vorticity in a warm blocking anticyclone. *Journal of the Atmospheric Sciences*, *41*, 3518–3526.

Legras, B., & Ghil, M. (1985). Persistent anomalies, blocking and variations in atmospheric predictability. *Journal of the Atmospheric Sciences*, *42*, 433–471.

Masato, G., Hoskins, B., & Woollings, T. (2013). Winter and summer Northern Hemisphere blocking in CMIP5 models. *Journal of Climate*, *26*, 7044–7059.

Matsueda, M. (2011). Predictability of Euro-Russian blocking in summer of 2010. *Geophysical Research Letters*, *38*, L06801. https://doi.org/10.1029/2010GL046557

Miralles, D. G., Teuling, A. J., Van Heerwaarden, C. C., & Vilà-Guerau de Arellano, J. (2014). Mega-heatwave temperatures due to combined soil desiccation and atmospheric heat accumulation. *Nature Geoscience*, *7*, 345–349.

Mullen, S. L. (1987). Transient eddy forcing of blocking flows. *Journal of the Atmospheric Sciences*, *44*, 3–22.

Nakamura, N., & Huang, C. S. Y. (2018). Atmospheric blocking as a traffic jam in the jet stream. *Science*, *361*, 42–47. https://doi.org/10.1126/science.aat0721

Nakamura, H., Nakamura, M., & Anderson, J. L. (1997). The role of high-and low-frequency dynamics in blocking formation. *Monthly Weather Review*, *125*, 2074–2093.

O'Reilly, C. H., Woollings, T., Zanna, L., & Weisheimer, A. (2018). The impact of tropical precipitation on summertime Euro-Atlantic circulation via a circumglobal wave-train. *Journal of Climate*, *31*, 6481–6504.

Pfahl, S., Schwierz, C., Croci-Maspoli, M., Grams, C., & Wernli, H. (2015). Importance of latent heat release in ascending air streams for atmospheric blocking. *Nature Geoscience*, *8*, 610–614.

Rex, D. F. (1950). Blocking action in the middle troposphere and its effect upon regional climate. I. An aerological study of blocking action. *Tellus*, *2*, 196–211.

Rivière, G., & Orlanski, I. (2007). Characteristics of the Atlantic storm-track eddy activity and its relation with the North Atlantic Oscillation. *Journal of the Atmospheric Sciences*, *64*, 241–266.

Russo, S., Sillmann, J., & Fischer, E. M. (2015). Top ten European heatwaves since 1950 and their occurrence in the coming decades. *Environmental Research Letters*, *10*, 124003.

Sanders, F., & Gyakum, J. R. (1980). Synoptic-dynamic climatology of the "bomb". *Monthly Weather Review*, *108*, 1589–1606.

Schaller, N., Sillmann, J., Antsey, J., Fischer, E. M., Grams, C., & Russo, S. (2018). Influence of blocking on Northern European and western Russian heatwaves in large climate models ensembles. *Environmental Research Letters*, *13*, 054015.

Schneidereit, A., Schubert, S., Vargin, P., Lunkeit, F., Zhu, X., Peters, D. H. W., & Fraedrich, K. (2012). Large-scale flow and the long-lasting blocking high over Russia: Summer 2010. *Monthly Weather Review*, *140*, 2967–2981.

Sousa, P. M., Trigo, R. M., Barriopedro, D., Soares, P. M. M., & Santos, J. A. (2018). European temperature responses to blocking and ridge regional patterns. *Climate Dynamics*, *50*, 457–477.

Uppala, S. M., Kållberg, P. W., Simmons, A. J., Andrae, U., Da Costa Bechtold, V., Fiorino, M., et al. (2005). The ERA-40 re-analysis. *Quarterly Journal of the Royal Meteorological Society*, *131*, 2961–3012.

Woollings, T., Barriopedro, D., Methven, J., Son, S.-W., Martius, O., Harvey, B., et al. (2018). Blocking and its response to climate change, *Current Climate Change Reports*, *4*, 287–300.